Geophys. J. Int. (2008) **175,** 417–432 doi: 10.1111/j.1365-246X.2008.03922.x

The design of an optimal filter for monthly GRACE gravity models

R. Klees,[1] E. A. Revtova,[1] B. C. Gunter,[1] P. Ditmar,[1] E. Oudman,[1] H. C. Winsemius[2] and H. H. G. Savenije[2]

[1] *Delft Institute of Earth Observation and Space Systems (DEOS), Delft University of Technology, Delft, the Netherlands. E-mail: B.C.Gunter@tudelft.nl*
[2] *Department of Water Resources Management, Delft University of Technology, Delft, the Netherlands*

Accepted 2008 July 17. Received 2008 July 17; in original form 2008 May 30

SUMMARY

Most applications of the publicly released Gravity Recovery and Climate Experiment monthly gravity field models require the application of a spatial filter to help suppressing noise and other systematic errors present in the data. The most common approach makes use of a simple Gaussian averaging process, which is often combined with a 'destriping' technique in which coefficient correlations within a given degree are removed. As brute force methods, neither of these techniques takes into consideration the statistical information from the gravity solution itself and, while they perform well overall, they can often end up removing more signal than necessary. Other optimal filters have been proposed in the literature; however, none have attempted to make full use of all information available from the monthly solutions. By examining the underlying principles of filter design, a filter has been developed that incorporates the noise and full signal variance–covariance matrix to tailor the filter to the error characteristics of a particular monthly solution. The filter is both anisotropic and non-symmetric, meaning it can accommodate noise of an arbitrary shape, such as the characteristic stripes. The filter minimizes the mean-square error and, in this sense, can be considered as the most optimal filter possible. Through both simulated and real data scenarios, this improved filter will be shown to preserve the highest amount of gravity signal when compared to other standard techniques, while simultaneously minimizing leakage effects and producing smooth solutions in areas of low signal.

Key words: Satellite geodesy; Time variable gravity; Hydrology.

1 INTRODUCTION

The Gravity Recovery and Climate Experiment (GRACE), launched in 2002, has provided the scientific community with valuable information regarding the time variable nature of the Earth's gravity field. The products available to the public range from the raw instrument measurements to the more refined products such as the u8mean and monthly spherical harmonic solutions. Even these monthly harmonic solutions require a certain degree of processing on the part of the user in order to realize their full potential. This is due to the fact that these monthly solutions are the output of a parameter estimation process, and are still subject to a range of random and systematic errors that are inherent to the instrument data and background models used. These errors increase rapidly with the spherical harmonic degree. The simplest way to suppress them is to truncate the spherical harmonic series around degree, say, 20–30. This approach, however, reduces dramatically the spatial resolution of the models. For applications in which high spatial resolution is desired, such as the monitoring of hydrological cycles at the basin level, the unaltered monthly GRACE solutions often contain too much noise to determine these regional signals accurately.

One approach to deal with noise in the GRACE monthly solutions is to apply a spatial averaging filter, with the idea that localized noise signals can be sufficiently attenuated by taking a weighted average of neighbouring points. The number of points to be included in the averaging process is dependent on the noise covariance structure. For the GRACE solutions, a number of averaging filters have already been proposed, ranging from simple isotropic Gaussian filters to more sophisticated anisotropic filters (e.g. Wahr *et al.* 1998; Chen *et al.* 2006; Swenson & Wahr 2006; Kusche 2007; Sasgen *et al.* 2006; Wouters & Schrama 2007; Davis *et al.* 2008). Each of these filters has its respective advantages and disadvantages. Some work better than others with a given type of noise. One example is the effectiveness of certain filters in suppressing the north–south 'stripes' common to most monthly solutions, caused by the reduced observability of the sectorial and near-sectorial coefficients from GRACE's polar orbit configuration. The destriping approach outlined by Swenson & Wahr (2006) is effective at removing these types of noise artefacts; however, in regions where such stripes do not exist, this filter may actually remove more gravity signal than other filters.

A completely different approach to deal with the noise in GRACE monthly gravity models is suggested by Han & Ditmar (2008) and

successfully applied to the Sumatra–Andaman earthquake by Han & Simons (2008). They propose a spatiospectral localization method, which suppresses the errors in the GRACE monthly gravity models yielding improved signal-to-noise ratio over a particular geographical region. The localization involves the multiplication of the estimated mass change function by a spatial band-limited window (isotropic) function centred at the region of interest. The window function is determined such that most of its energy is concentrated inside the region of interest.

The various filters available can be further divided into those filters that can be independently applied (i.e. they do not rely upon information about the signal and noise covariance structure), and so-called 'optimal' filters, which rely upon information about the expected signal and the errors in the Stokes coefficients. As an example, a basic implementation of the Gaussian filter is generic enough that it can be applied directly to any of monthly solutions without modification. Filters in the first category include the destriping approach by Swenson & Wahr (2006), and the empirical orthogonal function (EOF) approach developed by Wouters & Schrama (2007). The benefit to these filters is that the technique can be consistently applied to the solutions, and is not dependent on any sort of *a priori* information or error model. In addition, their implementation is often relatively simple, which makes it an attractive option for many users. On the contrary, the optimal filters rely on the principle that external knowledge of the problem (such as physical boundaries, solution error estimates, etc.) can be used to guide the filter in deciding what is noise and what is signal. The primary assumption here is that the external information used is both sufficiently accurate and reliable. Both categories of filters have their merits, but one of the goals of this paper is to argue that the filter that works best under most conditions is an optimal filter that relies on the expected signal in terms of Stokes coefficients and their error estimates, which are provided by the estimation process. This concept will be developed from the basic principles of the design of a filter, and will be supported by both simulated and real data scenarios. The approach to be outlined in this paper has the following properties.

(i) The filter seeks to minimize a clearly defined objective function.

(ii) The filter makes use of the full variance–covariance matrix of errors in the solution. To date, this has not been incorporated into any other filter, but is essential because it utilizes the full set of correlations between the errors.

(iii) The filter makes use of information about the signal variance in the spatial domain, in contrast to other filters suggested in literature, which rely on information about the signal variance in the frequency domain.

(iv) The filter is both anisotropic and non-symmetric, making it capable of removing noise artefacts of an arbitrary shape, such as stripes.

(v) The filter can either be integrated into the processing of GRACE data directly, or it can be used as a post-processing filter, that is, both implementations of the filter generate identical results.

These properties result in a filter that preserves signal better than any other filter tested and performs well everywhere. This is achieved because the approach developed reduces 'leakage' to and from areas outside the region of interest, and suppresses noise much stronger in regions of low signal (i.e. oceans, deserts, etc.). Examples from controlled simulations, as well as applications using real GRACE data on selected basins where the ground truth values are well known, will be shown to demonstrate this improved performance. The simulations will test the performance of a range of filters on both longitudinally and latitudinally oriented signals, with and without artificial noise added. The basins tested for the real data cases include the Zambezi river basin, for which a detailed and accurate hydrology model exists (see Winsemius *et al.* 2006), as well as the Sahara desert, where the hydrology signal should be close to zero.

2 OPTIMAL FILTER DESIGN

Suppose f is the mass change function (expressed in units of equivalent water height) and f_w is the filtered mass change function; $\hat{f}$ and $\hat{f}_w$ are the corresponding quantities as inferred from GRACE data. We assume that these functions are defined on the surface of the mean Earth sphere σ_R with radius R. From this we can say that f is related to f_w in the following way:

$$f_w(x) = \frac{1}{4\pi R^2} \int_{\sigma_R} f(y)\, W(x, y)\, \mathrm{d}\sigma_R(y), \tag{1}$$

where $W(x, y)$ is the filter function and x and y denote points on the mean Earth sphere with radius R. The same relation exists between the estimates $\hat{f}_w$ and $\hat{f}$. The most general filter function is a two-point function on the sphere σ_R,

$$W(x, y) = \sum_{l,m} \sum_{p,q} W_{lm,pq}\, \bar{Y}_{l,m}(\xi)\, \bar{Y}_{p,q}(\eta), \quad \xi = \frac{x}{|x|},\ \eta = \frac{y}{|y|}, \tag{2}$$

where l and m are degree and order, $\bar{Y}_{l,m}$ are the 4π-normalized (or fully normalized) spherical surface harmonics, $W_{lm,pq}$ are the filter coefficients, and ξ and η are points on the unit sphere. The filter function $W(x, y)$ is (i) anisotropic as it depends on degree and order, and (ii) non-symmetric with respect to the points x and y. Therefore, we call this filter an 'anisotropic, non-symmetric filter', or simply the ANS filter for short.

To determine the values of the filter coefficients, a wide range of objective functions can be used. The filter we pursue minimizes the global mean of the mean-square error (MSE), that is, it minimizes

$$\mathrm{MSE}_{\mathrm{ave}} = \frac{1}{4\pi R^2} \int_{\sigma_R} E\{(f - \hat{f}_w)^2\}\, \mathrm{d}\sigma_R, \tag{3}$$

where $E\{\cdot\}$ is the statistical expectation operator. Hence, the filter we look for minimizes the global mean of the mean square difference between the actual (unfiltered) mass change function f and the filtered mass change function as inferred from GRACE data, $\hat{f}_w$. We call this filter the 'optimal ANS filter'. A straightforward computation reveals that the minimizer of $\mathrm{MSE}_{\mathrm{ave}}$ is

$$\mathbf{W} = \mathbf{D}\,(\mathbf{C} + \mathbf{D})^{-1}. \tag{4}$$

$\mathbf{W} = (W_{lm,pq})$ is the filter matrix and the filter coefficients are arranged in such a way that each pair (l, m) defines one particular row of $\mathbf{W}$; $\mathbf{C}$ is the full noise variance–covariance matrix of the Stokes coefficients of the estimated mass change function $\hat{f}$, that is,

$$\mathbf{C} = (c_{lm,pq});\ c_{lm,pq} = E\left\{\bar{c}_{l,m}^{(\varepsilon f)} \bar{c}_{p,q}^{(\varepsilon f)}\right\}, \tag{5}$$

where $\bar{c}_{l,m}^{(\varepsilon f)}$ are the Stokes coefficients of the error $\varepsilon_f = f - \hat{f}$; $\mathbf{D}$ is the matrix with elements

$$\mathbf{D} = (d_{lm,pq});\ d_{lm,pq} = \bar{c}_{l,m}^{(f)} \bar{c}_{p,q}^{(f)}, \tag{6}$$

where $\bar{c}_{l,m}^{(f)}$ are the Stokes coefficients of the mass change function f. We call $\mathbf{D}$ the (frequency-domain) signal variance–covariance matrix. Note that when the mass change function is interpreted as

a random function on the sphere, the entries of the matrix **D** are defined as

$$d_{lm,pq} = E\left\{\bar{c}^{(f)}_{l,m}\bar{c}^{(f)}_{p,q}\right\}. \tag{7}$$

It can be shown easily that the application of the optimal ANS filter is equivalent to applying some regularization to the GRACE normal equations. To show this, we re-arrange eq. (4) to obtain

$$\begin{aligned}\mathbf{D}\,(\mathbf{C}+\mathbf{D})^{-1} &= (\mathbf{C}\mathbf{D}^{-1}+\mathbf{D}\mathbf{D}^{-1})^{-1}\\ &= (\mathbf{C}\mathbf{D}^{-1}+\mathbf{I})^{-1}\\ &= (\mathbf{C}\mathbf{D}^{-1}+\mathbf{C}\mathbf{C}^{-1})^{-1}\\ &= (\mathbf{C}^{-1}+\mathbf{D}^{-1})^{-1}\,\mathbf{C}^{-1}.\end{aligned} \tag{8}$$

If we let $\mathbf{N}\,\hat{\mathbf{x}} = \mathbf{b}$ denote the normal equations associated with a least-squares adjustment of GRACE K-band ranging (KBR) data, that is, $\mathbf{C} = \mathbf{N}^{-1}$, and we let $\hat{\mathbf{x}}_w$ represent the vector of filtered Stokes coefficients, we can write

$$\hat{\mathbf{x}}_w = \mathbf{W}\,\hat{\mathbf{x}} = \mathbf{D}\,(\mathbf{C}+\mathbf{D})^{-1}\,\hat{\mathbf{x}} \tag{9}$$

$$\begin{aligned}&= (\mathbf{C}^{-1}+\mathbf{D}^{-1})^{-1}\,\mathbf{C}^{-1}\,\hat{\mathbf{x}}\\ &= (\mathbf{N}+\mathbf{D}^{-1})^{-1}\,\mathbf{N}\,\hat{\mathbf{x}} = (\mathbf{N}+\mathbf{D}^{-1})^{-1}\,\mathbf{b}.\end{aligned} \tag{10}$$

Hence, filtering the Stokes coefficients with an optimal ANS filter is identical to a regularized least-squares adjustment of GRACE KBR data if the regularization matrix is equal to the inverse signal variance–covariance matrix. Therefore, the optimal ANS filter of eq. (4) is a regularization-type filter. Such a filter has already been discussed in (Kusche 2007).

Several modifications can be applied to obtain filters, which have a simpler structure than the general ANS filter. For instance, we may require that the filter function has the following spherical harmonic representation

$$W(x,y) = \sum_{l,m} W_{l,m}\,\bar{Y}_{l,m}(\xi)\,\bar{Y}_{l,m}(\eta). \tag{11}$$

This filter function is symmetric with respect to the points x and y but it is still anisotropic. We call this an 'anisotropic symmetric' filter, or an 'AS filter' for short.

The AS filter that minimizes $\mathrm{MSE}_{\mathrm{ave}}$ is the 'optimal' AS filter; a straightforward computation reveals that the corresponding filter matrix **W** is diagonal with elements

$$W_{l,m} = \frac{d_{lm,lm}}{d_{lm,lm}+c_{lm,lm}}. \tag{12}$$

Obviously, when forcing the filter function to have the structure of eq. (11), the minimum of $\mathrm{MSE}_{\mathrm{ave}}$ is independent of (frequency-domain) signal covariances and noise covariances.

The most simple filter function is

$$W(x,y) = \sum_{l,m} W_l\,\bar{Y}_{l,m}(\xi)\,\bar{Y}_{l,m}(\eta). \tag{13}$$

We call this an 'isotropic symmetric' (IS) filter. For the IS filter, $\mathrm{MSE}_{\mathrm{ave}}$ attains a minimum if

$$W_l = \frac{\sum_m d_{lm,lm}}{\sum_m d_{lm,lm}+\sum_m c_{lm,lm}} = \frac{\sigma_l^2(f)}{\sigma_l^2(f)+\sigma_l^2(\varepsilon_f)}, \tag{14}$$

where $\sigma_l^2(f)$ and $\sigma_l^2(\varepsilon_f)$ denote the signal degree variances and noise degree variances, respectively. The filter matrix associated with the optimal IS filter is a diagonal matrix, and the diagonal elements only depend on the spherical harmonic degree. Note that the application of an optimal AS filter or an optimal IS filter cannot be interpreted anymore as a regularized least-squares solution of GRACE data, because both filters do not make use of the full normal equation matrix. AS-type filters and IS-type filters have been suggested by many authors, though the objective function they minimize is different, unknown, or simply does not exist (e.g. Wahr *et al.* 1998; Swenson & Wahr 2002; Han *et al.* 2005; Swenson & Wahr 2006; Seo *et al.* 2006). If an objective function does not exist, the filter coefficients have to be determined in another way. This is done either by trial-and-error, the application of other statistical optimization principles, or the comparison with independent geophysical data.

3 PRACTICAL ASPECTS OF ANS FILTER DESIGN

The optimal ANS filter of eq. (4) exploits information about the signal and noise variance–covariance matrices. The latter can be computed if the normal equation matrix, **N**, is available. However, normal equation matrices or, equivalently, noise variance–covariance matrices, are not an official standard level 2 product, and so far, access to them is limited to the teams, which compute GRACE models from GRACE KBR data. The majority of the scientific community only has access to the noise variances. For that reason, Kusche (2007) proposed to use an approximate noise variance–covariance matrix, which only requires publicly available information about the GRACE orbit geometry. The corresponding filter is a simplified version of the optimal ANS filter in two respects: (1) it uses a synthetic noise variance–covariance matrix, which is based on the assumption that the noise in potential differences between the two GRACE satellites is white and (2) it uses a diagonal signal variance–covariance matrix following a power law in the spherical harmonic degrees. These assumptions may be critical in two respects: (1) the noise correlations are not modelled properly (remember that destriping is effective because it mimics the dominant feature of noise correlations) and (2) signal correlations in the spherical harmonics domain are completely ignored. A sensitivity study to be presented in 6 will answer the question whether these assumptions lead to a filter which performs similar to the optimal ANS filter.

Another problem of optimal ANS filter design is the computation of the entries of the signal variance–covariance matrix **D**, eq. (4). One possibility is to construct a mass change function using geophysical models of ocean mass redistribution and terrestrial water storage variations. They may be taken from the multi-institutional Estimating the Circulation and Climate of the Ocean (ECCO) project (Fukumori *et al.* 2000), the Global Land Data Assimilation System (GLDAS) (Rodell *et al.* 2004), or the Land Dynamics (LaD) model (Milly & Shmakin 2002) to name a few. When we assume that I monthly mean models of ocean mass redistribution and terrestrial water storage variations are available, we could consider them as I realizations of the mass change function and could compute estimates of the elements of the matrix **D** by averaging the products $\bar{c}^{(f)}_{l,m}\,\bar{c}^{(f)}_{p,q}$ over I months. We made a series of experiments following this approach and always obtained filters of very poor quality. To our understanding, this is caused by the presence of strong global signal correlations, in particular seasonal variations, implying the signal behaviour is not random at all. An approach often seen in the literature is to compute signal degree variances from geophysical models, or GRACE monthly gravity models, and neglect all covariances in the spherical harmonics domain (e.g. Seo *et al.* 2006; Kusche 2007). That is, the full signal–covariance matrix **D** is approximated by a diagonal matrix and the diagonal entries depend only on the spherical harmonic degree. Note that a

diagonal signal variance–covariance matrix **D** propagates into a full signal variance–covariance matrix in the spatial domain, according to the spherical harmonic synthesis relations. Therefore, the statement in (Kusche 2007) that his ANS filter uses a full signal variance–covariance matrix should be understood as a full signal variance–covariance matrix in the spatial domain, whereas this matrix is diagonal in the frequency domain.

We propose an alternative way of computing the frequency-domain signal variance–covariance matrix **D**. Suppose that I models of monthly mean mass variations are available (how to get them will be discussed later). From them we compute the signal variance at a set of K suitably chosen points on the entire mean Earth sphere. The signal covariances between these points are neglected. The points may be the nodes of an equal-angular grid or may belong to any homogeneous point distribution on the sphere (e.g. Freeden *et al.* 1998). These variances form the elements of the diagonal spatial-domain signal variance–covariance matrix **F**. From **F**, the frequency-domain signal variance–covariance matrix **D** is computed by error propagation using the spherical harmonic analysis relation

$$\bar{c}_{l,m}^{(f)} = \frac{1}{4\pi R^2} \int_{\sigma_R} f\, \bar{Y}_{l,m}\, \mathrm{d}\sigma_R \approx \sum_{k=1}^{K} f_k\, \bar{Y}_{l,m;k}\, w_k, \tag{15}$$

where f_k is the mass change at node k, $\bar{Y}_{n,m;k}$ is the spherical surface harmonic of degree l and order m at node k, and w_k are suitably chosen cubature weights. Eq. (15) can be written in matrix-vector notation as

$$\mathbf{d} = \mathbf{Y}\,\mathbf{f}, \tag{16}$$

where $\mathbf{d}$ is the $L \times 1$ vector of Stokes coefficients $\{\bar{c}_{l,m}^{(f)}\}$, $\mathbf{Y}$ is the $L \times K$ matrix with elements $\bar{Y}_{l,m;k}\, w_k$, L is the number of Stokes coefficients of the GRACE model, and $\mathbf{f}$ is the $K \times 1$ vector of function values f_k. Then, according to the law of covariance propagation, we obtain

$$\mathbf{D} = \mathbf{Y}\,\mathbf{F}\,\mathbf{Y}^T. \tag{17}$$

Note that the matrix **D** built up in this way is a full matrix. Nevertheless, it is just an approximation to the 'real' frequency-domain signal variance–covariance matrix, because spatial-domain signal covariances have been neglected. The nodes and weights could be taken from a cubature formula on the sphere. The most simple choice is to select K points on the sphere, and to choose the weights according to

$$w_k = \frac{4\pi R^2}{K}. \tag{18}$$

More accurate cubature formulas are known, but for the purpose of optimal ANS filter design, numerical integration errors are not critical. If the nodes are located on an equal-angular grid, fast Fourier transform (FFT) methods can be used to evaluate the expression of eq. (17) efficiently (e.g. Healy *et al.* 2003).

Unfortunately, the signal variance–covariance matrix obtained according to eq. (17) yields signal variances per coefficient, which are constant. This follows immediately from eq. (15):

$$\begin{aligned} \tfrac{1}{2l+1} \sum_m \left| c_{l,m}^{(f)} \right|^2 &\approx \frac{1}{2l+1} \sum_{i,k} f_i f_k\, w_i w_k \sum_m \bar{Y}_{l,m;i}\, \bar{Y}_{l,m;k} \\ &= \sum_{i,k} f_i f_k\, w_i w_k\, P_{l;ik} = \text{constant}. \end{aligned} \tag{19}$$

Therefore, any attempt to directly use such a signal variance–covariance matrix fails. As a solution, we propose to apply an additional scaling of the signal covariances according to

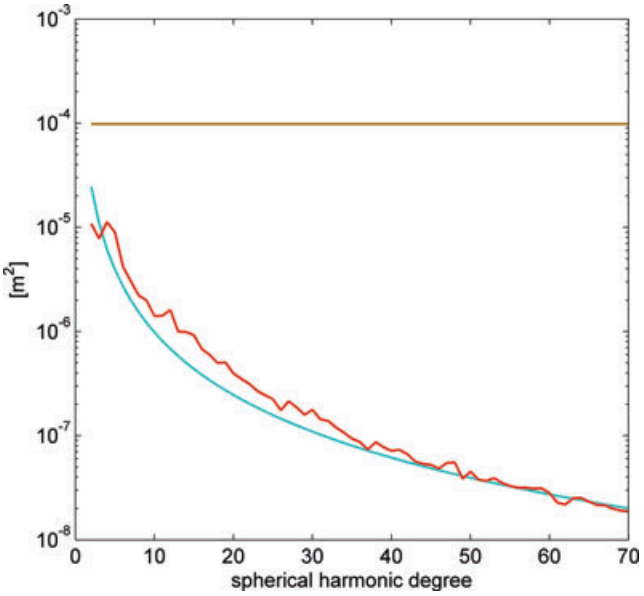

Figure 1. Mean signal variances per coefficient in terms of equivalent water height before scaling (brown) and after scaling (blue) according to eqs (20) and (21). The latter fit rather well the mean signal variances per coefficient of a combined ECCO/GLDAS model (red).

$$\mathbf{D} \approx \mathbf{S}\mathbf{Y}\,\mathbf{F}\,\mathbf{Y}^T\,\mathbf{S}, \tag{20}$$

where **S** is a diagonal matrix with entries

$$\mathbf{S} = (s_{lm,lm}) = \begin{cases} 1 & l = 0 \\ \frac{1}{l} & \text{otherwise} \end{cases}. \tag{21}$$

The corresponding mean signal variances per coefficient match the spectrum of the mass change function rather well, as depicted in Fig. 1. Note that such a scaling can be interpreted as an additional low-pass filtering; that is, instead of eq. (16), we use

$$\mathbf{d} = \mathbf{S}\,\mathbf{Y}\,\mathbf{f}. \tag{22}$$

It has not been addressed yet, how information about the signal is obtained to construct the signal variance–covariance matrix according to the procedure outlined above. The preferred source of information about the signal are geophysical models (e.g. Seo *et al.* 2006; Kusche 2007). However, as shown by Klees *et al.* (2007), the filtered solution will be biased towards these models. Therefore, we propose an alternative approach, which exclusively uses monthly GRACE gravity models to build the signal variance–covariance matrix iteratively. The iterations are initialized by assuming constant signal variances at an equal-angular grid. That is, the initial matrix **F** is a scaled unit matrix. Then, an initial matrix **D** is computed using eq. (20), the ANS filter is designed according to eq. (4), and the Stokes coefficients of I monthly GRACE fields are filtered. These I sets of filtered Stokes coefficients represent monthly signals and are used in the next iteration to compute the signal variances at the K nodal points, to compute a new matrix **D**, and to design a new ANS filter. The iterations stop if the differences between two sets of filtered Stokes coefficients are below a given threshold. Fig. 2 shows an example of the signal amplitudes (i.e. the square root of the signal variances) from 36 monthly GRACE models spanning the period 2003 February till 2006 February after two iterations have been performed. The iterations were initialized assuming a homogeneous signal amplitude of 5 cm. Note that the result is quite

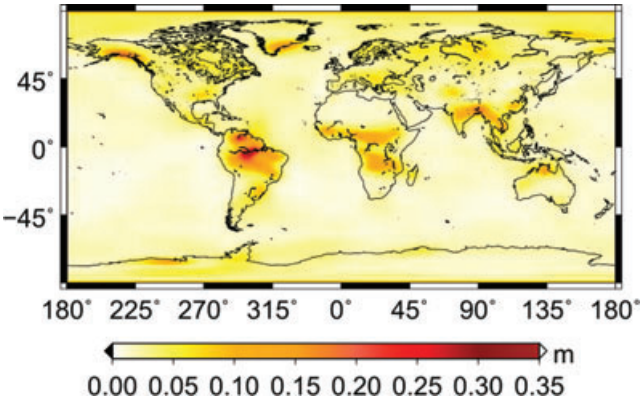

Figure 2. Signal amplitudes computed from 36 monthly GRACE models after two iterations in units of [m] equivalent water heights; the initial signal amplitudes were set equal to 5 cm. The signal variances form the entries of the diagonal spatial-domain signal covariance function **F** of eq. (17), which is used to design the optimal ANS filter.

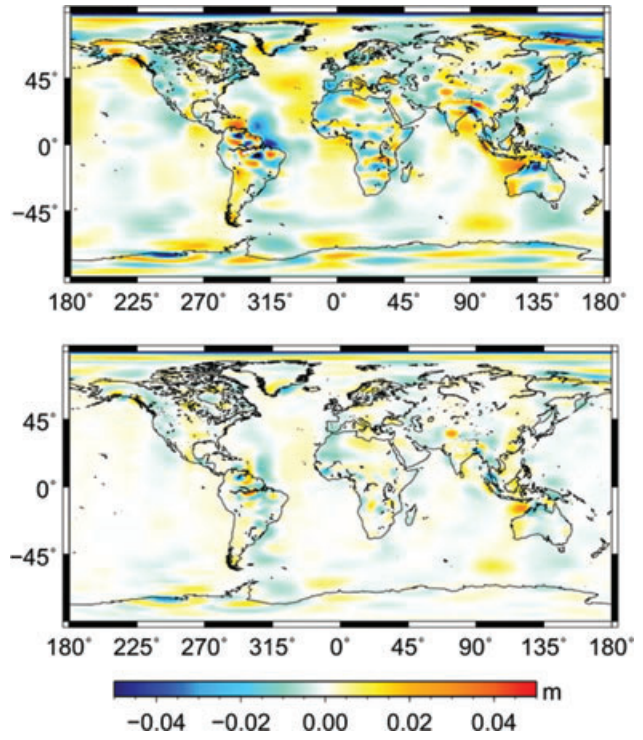

Figure 3. Difference between two filtered GRACE solutions for 2005 April. Top panel: initial-filter solution minus first-iteration-filter solution. Bottom panel: first-iteration-filter solution minus second-iteration-filter solution. The results indicate a fast convergence of the iterative ANS filter design scheme.

robust against the choice of the initial signal variances as shown in all experiments. In this way, we compute the optimal ANS filter for each particular month. Each monthly optimal ANS filter uses the same signal variance–covariance matrix and the noise variance–covariance matrix of that particular month.

Fig. 3 depicts the differences between the initial filter and the filters after the first and second iteration. The initial filter was designed assuming that the mass change function is described by a constant water layer of 5 cm thickness over the globe. The differences do not exceed 4 and 2 cm, respectively. A similar rapid convergence has been observed in many practical tests; not more than three iterations were needed.

4 FILTER PERFORMANCE – SIMULATIONS

In order to understand how the optimal ANS filter behaves and to assess its performance, we apply the filter to three simulated data sets. Four filters are included in the comparison: a 700 km isotropic Gaussian filter (G700), the convolution of the destriping filter with a 400 km isotropic Gaussian filter (DS400), the optimal AS filter (AS), and the optimal ANS filter (ANS).

We first consider an isolated target area, which extends 2000 km in north–south direction and 500 km in east–west direction. The target area has been centred at 0° latitude and 20° longitude. Note that the choice of the longitude is completely arbitrary; however, the choice of the latitude matters as GRACE solution errors strongly depend on the latitude. Note further that a real GRACE solution (DEOS Stokes coefficients for 2005 April) has been used to define the destriping parameters of the DS400 filter; moreover, the same solution and the associated variance–covariance matrix have been used to design the optimal AS filter, and the optimal ANS filter. The mass change function (signal) to be recovered is the spherical harmonic degree 70 representation of a 10 cm water layer homogeneously distributed over the target area. The filters are directly applied to this signal. The destriping filter uses a degree 3 Savitzky-Golay smoothing filter (Savitzky & Golay 1964) over a 7-point window; orders below eight were left unchanged. The spatial-domain signal amplitudes used to construct the signal covariance matrix **D** are set equal to 5 cm. No iterations were performed to improve the filters in order to avoid the situation that the optimal AS filter and the optimal ANS filter use any information about the true signal. North–south and east–west cross-sections of the G700, AS, and ANS filter functions are shown in Fig. 4. Note the negative lobes of the AS filter and the ANS filter close to the filter centre, which are needed to reduce the correlated noise. Moreover, the optimal AS and optimal ANS filter functions have smaller half widths in north–south direction as the G700 filter. The amplitudes of the side-lobes of the ANS filter are much larger than the side-lobes of the AS filter; they attain about 40 per cent of the amplitude of the main lobe, whereas this value is below 10 per cent for the AS filter. The filter half widths differ significantly. In north–south direction, the ANS always has the smallest half width (about 330 km in the left-hand panel of Fig. 4), followed by the AS filter (400 km) and the G700 filter (700 km). In the east–west direction, however, the AS-filter half width is significantly larger than 700 km (950 km in the right-hand panel of Fig. 4), whereas the ANS filter has again the smallest half width (520 km). It is also remarkable that the ANS filter does not take up its maximum value at exactly the computation point. In fact, it is shifted by about 110 km to the north.

Fig. 5 shows the signal before and after filtering has been applied. The G700 filter is isotropic, which is the reason why we obtain rounded contours deviating from the true basin shape as evident in Fig. 5. The DS400 filter has negative lobes close to the centre of the filter to reduce the strong noise correlations in the sectorials. They are responsible for the clearly visible negative leakage signal north and south to the target area. The convolution of the destriping filter with a 400 km isotropic Gaussian filter is responsible for some rounded contours, which overlay the effects of destriping. The less pronounced negative lobes of the AS-filter in the north–south direction is an indication that the AS filter does not sufficiently

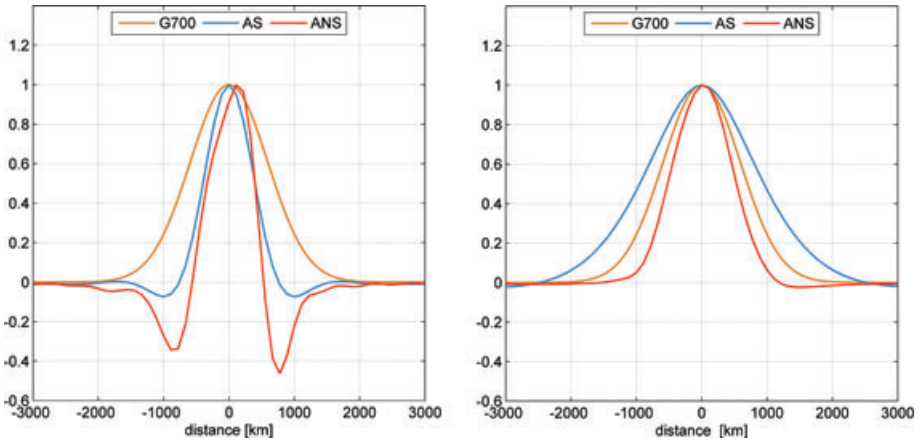

Figure 4. North–south (left-hand panel) and east–west (right-hand panel) cross-sections through the normalized filter functions G700, AS, and ANS. The filter functions are centred at 0° latitude and 20° longitude.

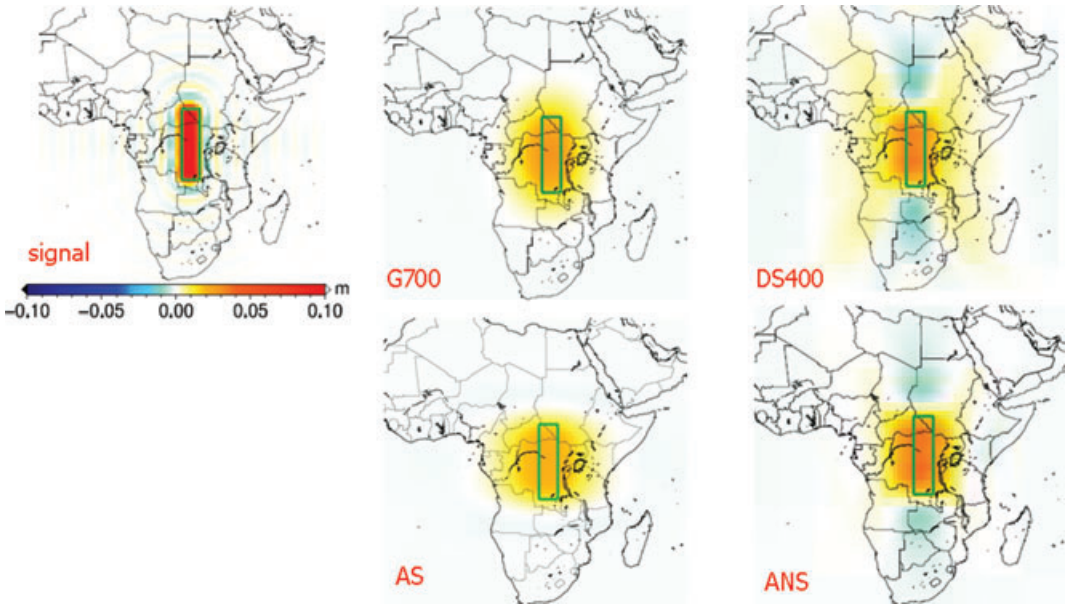

Figure 5. Isolated, north–south elongated target area with a 10-cm water mass layer before and after filtering. 700 km isotropic Gaussian filter (G700), convolution of destriping filter and 400 km isotropic Gaussian filter (DS400), optimal AS filter (AS) and optimal ANS filter (ANS). The non-zero signal outside the target area is the effect of filtering. Note the pretty strong negative signal to the north and south of the target area for the DS400 and ANS solutions, which is caused by the negative lobes of the filter functions close to the filter centre.

reduce the highly correlated noise in the Stokes coefficients. The optimal ANS filter takes the full noise correlations into account and shows similar leakage patterns in the north–south direction as the DS400 filter. The main difference to destriping is that the ANS filter takes all noise correlations into account, including the noise correlations in the near sectorials, which are not smoothed sufficiently well by destriping. Moreover, the optimal ANS filter also takes noise and signal correlations into account, which leads to a smaller half width in east–west direction than any other filter.

Next, we consider the same target area, but now rotated by 90°, that is, the area is now elongated in east–west direction. The G700 shows similar rounded contours as already observed for the north–south elongated target area, which had to be expected due to the isotropy of the filter (Fig. 6). All other filters behave differently. In particular, we observe that now leakage is significantly smaller than for the north–south elongated target area. Again, the ANS filter shows the lowest smearing in the east–west direction.

In the third example, we consider the same target area as in the first example, except we now assume that close to the target area there is another region of significant mass change (of opposite sign). More specifically, to the east of the target area, we assume a mass change signal of −10 cm covering an area of the same size as the target area (see Fig. 7). That is, the mass change signal in that area is completely out-of-phase with the mass change signal inside the target area. Fig. 7 shows that this scenario is a worst-case scenario for GRACE, because GRACE fails completely to recover the signal, no matter what filter is being used.

In order to better quantify the loss of signal over the target area, we computed the north–south and east–west cross-sections for each scenario (Figs 8 and 9) and the mean water mass change after filtering (Table 1). The loss of signal is the strongest for the non-isolated, north–south elongated target area; more than 90 per cent of the signal has been lost after filtering. The situation is significantly better for isolated target areas. The east–west elongated target area is

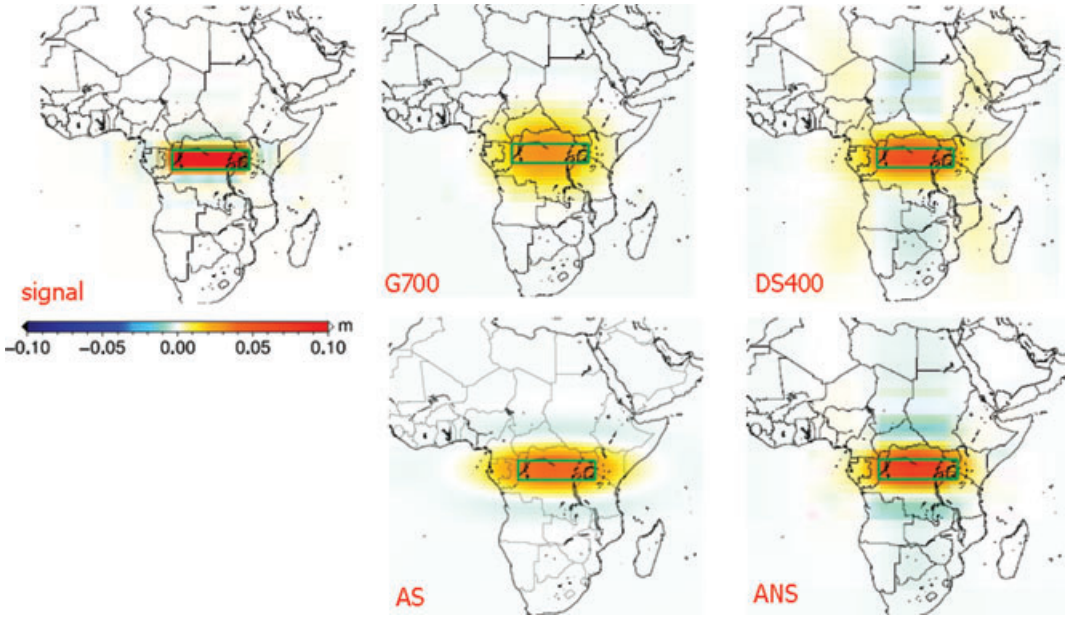

Figure 6. Isolated, north–south elongated target area with a 10-cm water mass layer before and after filtering. 700 km isotropic Gaussian filter (G700), convolution of destriping filter and 400 km isotropic Gaussian filter (DS400), optimal AS filter (AS) and optimal ANS filter (ANS). It is evident that leakage is less pronounced than for the north–south elongated target area shown in Fig. 5.

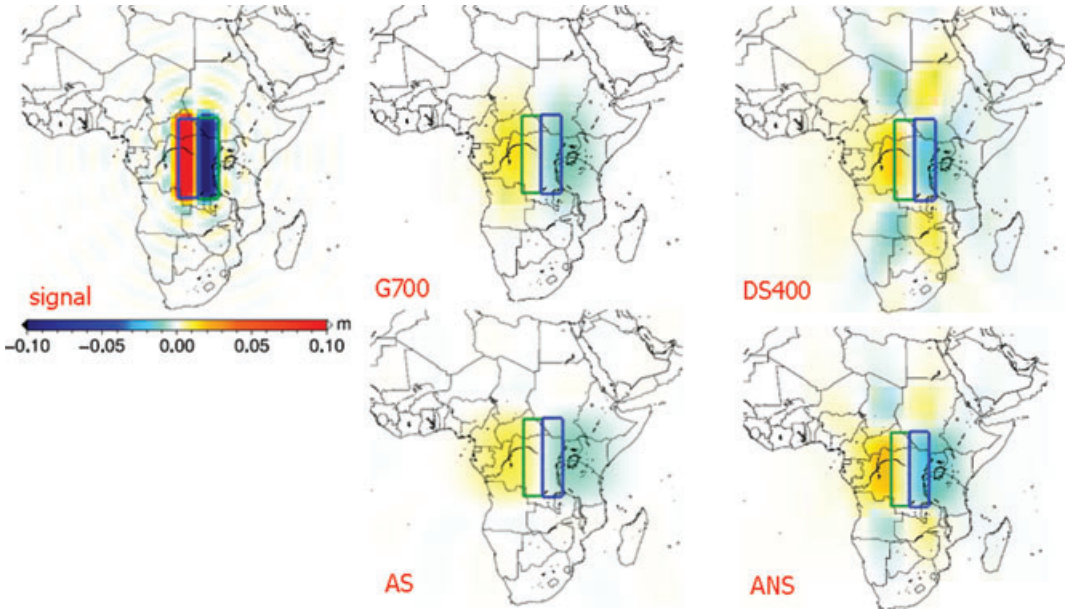

Figure 7. Non-isolated target area with a strong out-of-phase mass change signal of −10 cm to the east of the target area before and after filtering. 700 km isotropic Gaussian filter (G700), convolution of destriping filter and 400 km isotropic Gaussian filter (DS400), optimal AS filter (AS) and optimal ANS filter (ANS). This example shows the problem of any filter when there is a strong out-of-phase mass change signal close to the target area.

less affected than the north–south elongated one. Note that rescaling as suggested by Velicogna & Wahr (2006) can be applied no matter what filter is being used. Whether rescaling is helpful depends on how strong the signal is outside the target area. If it is significantly smaller than the signal inside the target area (ideally zero as for isolated target areas), then rescaling is an appropriate tool to improve the amplitude estimates. However, for non-isolated target areas with a strong out-of-phase signal in the neighbourhood of the target area, rescaling is no longer reliable. Instead, the procedure of Klees *et al.* (2007) has to be followed, which uses available information about the mass change function inside and outside the target area provided by GRACE or geophysical models.

In the second series of experiments, we want to investigate how the filters perform in terms of noise reduction. The full noise variance–covariance matrix of a GRACE solution for 2005 April computed at DEOS, complete to degree 70, has been used to generate several realistic realizations of noise in the Stokes coefficients $\bar{c}^{(\hat{f})}_{l,m}$. In the following, we show only one noise realization; all conclusions are valid for the other realizations, as well. The upper left-hand panel of Fig. 10 shows the spatial pattern of one

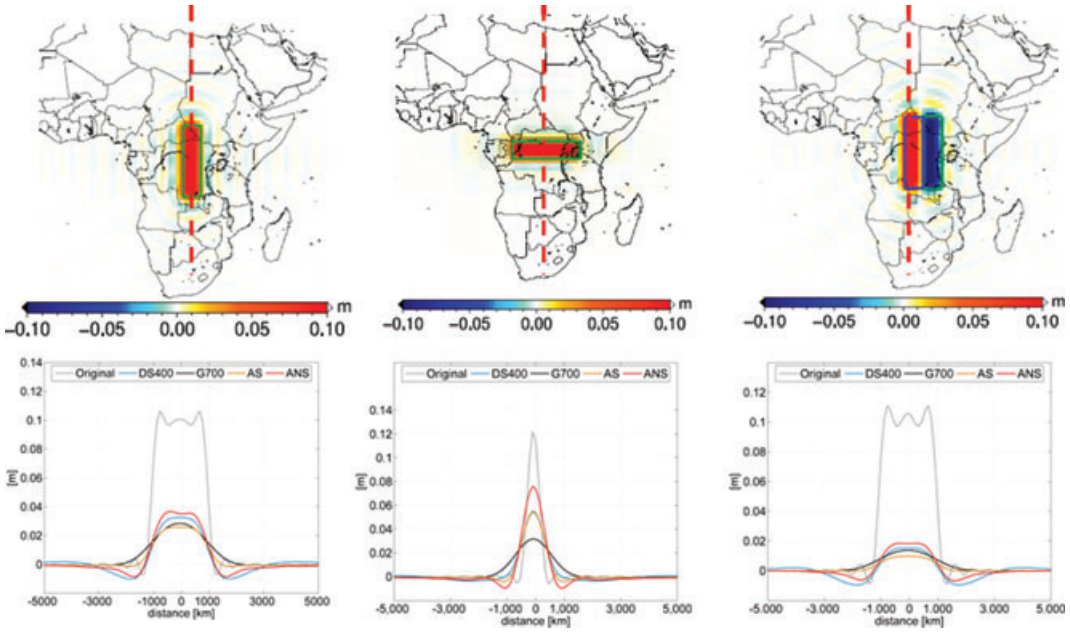

Figure 8. Original and filtered signal along north–south cross-sections through the three target areas. Note the strong loss of signal caused by the filters.

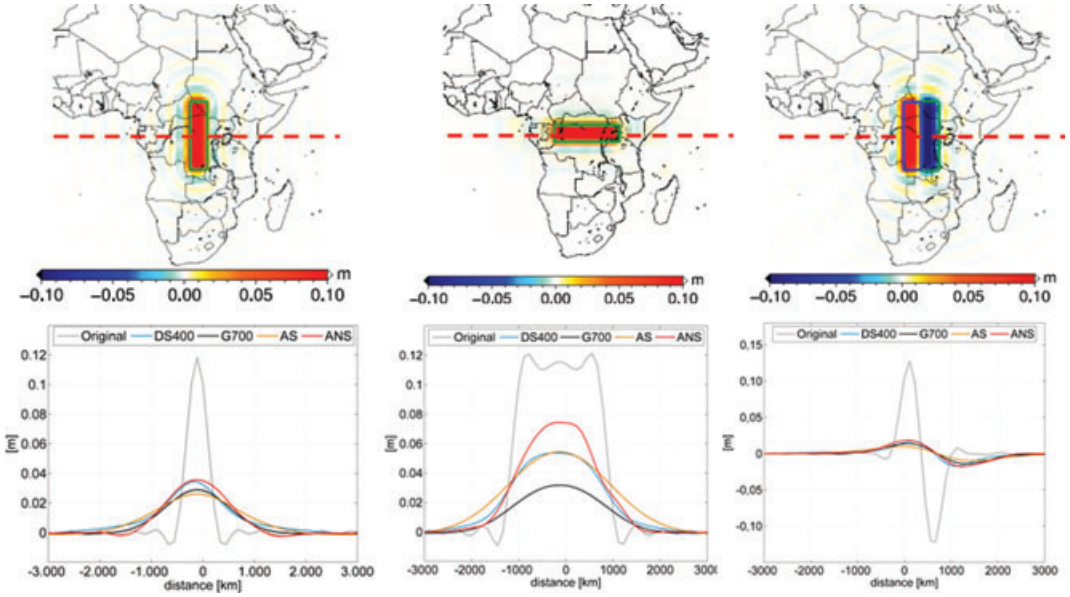

Figure 9. Original and filtered signal along east–west cross-sections through the three target area. There is no significant difference with respect to north–south cross-sections as shown in Fig. 8.

Table 1. Mean mass change over three target areas (each of size 1.1 × 10^6 km^2) in units of (m) after filtering. The exact value is 0.1 m.

Filter	Isolated north–south	Isolated east–west	Non-isolated north–south
G700	0.024	0.026	0.007
DS400	0.027	0.043	0.009
AS	0.023	0.044	0.004
ANS	0.031	0.056	0.009

particular noise realization. The pattern is dominated by the well-known north–south stripes. Note that the noise amplitudes take up values of 5 m. All filters succeed in reducing noise significantly by about two orders of magnitude. The application of the G700 filter gives the best smoothing. Due to the large half width of 700 km, noise is distributed smoothly over larger areas, which is the reason why the maximum amplitudes of noise artefacts are about a factor of 2 smaller than for the other filters. DS400 leaves significantly more noise in equatorial regions; this is well known and explained by the fact that noise is also strong in the near sectorial coefficients, which is not smoothed enough when destriping (Swenson & Wahr 2006). Fig. 10 demonstrates nicely how the optimal ANS filter works. When designing the filter, it was assumed that the signal variance is 0.75 cm on the oceans and 5.0 cm on land. Hence, the filter is more aggressive on the oceans, which is the reason for the very smooth and low amplitude residual noise pattern. On land, however, the smoothing is less pronounced as the filter expects a stronger signal. All other filters do not distinguish between areas

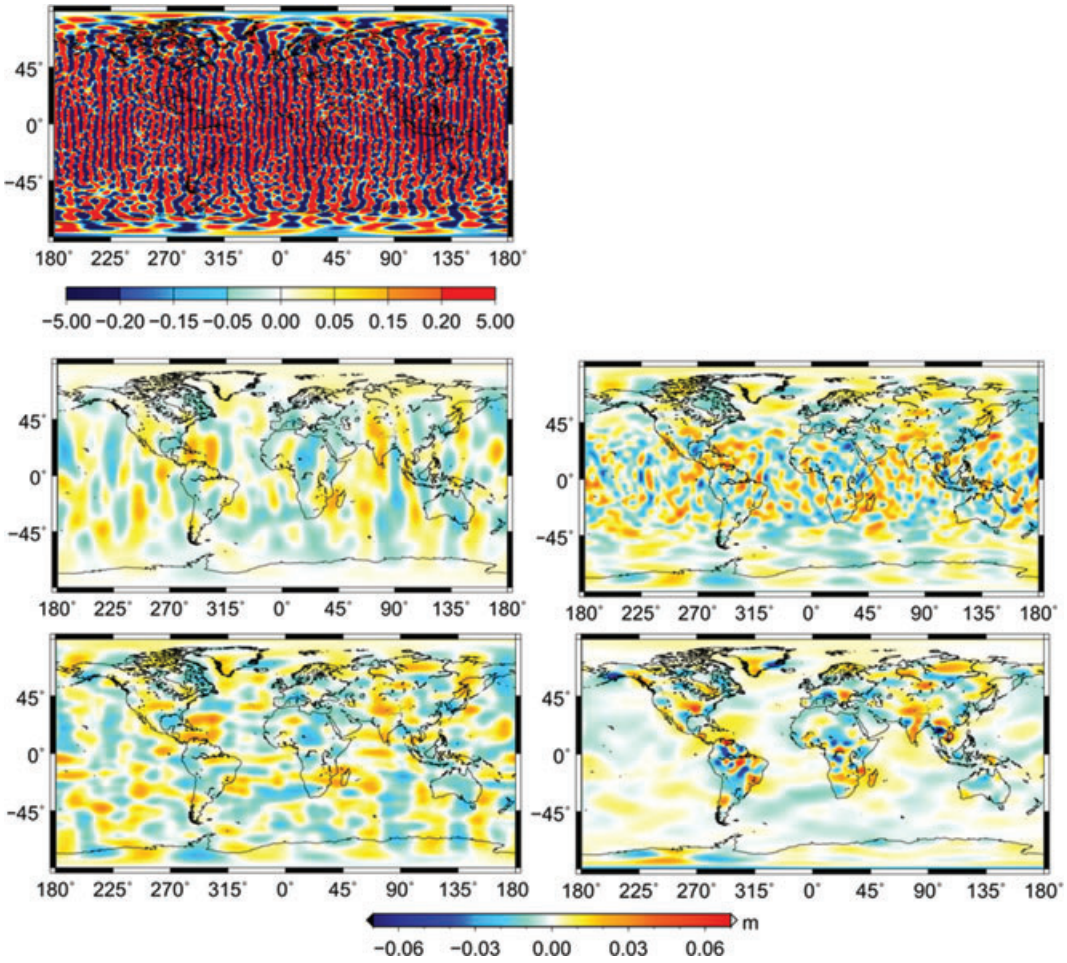

Figure 10. Noise before (left-hand upper panel) and after filtering. 700 km isotropic Gaussian filter (G700, left-hand middle panel), convolution of destriping filter and 400 km isotropic Gaussian filter (DS400, right-hand middle panel), optimal AS filter (AS, left-hand lower panel) and optimal ANS filter (ANS, right-hand lower panel). Filtering is a very efficient tool to reduce noise. Depending on what filter is being used, residual noise attains extreme amplitudes of 2–4 cm. G700 provides the smallest amplitudes and the smoothest map of residual noise. Note the very smooth result over the oceans when the optimal ANS filter is applied.

of different signal amplitudes. Finally, the ANS filter performs the same, independently of the latitude. It is also remarkable how different the optimal AS filter behaves compared with the optimal ANS filter. In particular, the residual noise left by the AS filter is quite homogeneous over the globe, and significantly higher on the oceans.

Fig. 11 shows a zoom-in of Fig. 10 to point to another aspect of correlated noise: the DS400 solution, optimal AS solution, and optimal ANS solution suffer from noise artefacts which extend over areas as large as 10^6 km^2 without changing the sign. Amplitudes attain values up to 4 cm. This means in fact that when computing the mean mass change over areas of comparable or smaller size, there is no guarantee that noise cancels out or is reduced significantly. Computing the mean mass change over a target area may reduce noise only if the target area is much larger than, say, 10^6 km^2. Note that spatial averaging hardly reduce noise after a G700 filter has been applied. This, however, is less critical as the residual noise amplitudes of a G700 solution are significantly smaller than for DS400, optimal AS and optimal ANS solutions. A practical implication of this result is that when using GRACE to quantify continental water cycling, it may be very difficult to decide whether a particular pattern of size 10^6 km^2 or smaller is residual noise or signal. This is confirmed by Fig. 12, which shows the sum of synthetic signal and noise after filtering. All patterns marked by red circles may be interpreted as signal, but are in fact noise artefacts. These noise artefacts pose a natural limit to the spatial resolution of monthly GRACE fields for land water cycling. Also the appealing mascon solutions (e.g. Rowlands *et al.* 2005) suffer from the same problem no matter whether regularization is applied or not. A time-series plot of each mascon may help to detect noise artefacts in that particular mascon. This approach is followed by Lemoine *et al.* (2007). However, episodic mass change events remain hard to distinguish from noise artefacts.

5 FILTER PERFORMANCE – REAL DATA

Another series of computations is done using real data. Two target areas will be considered in more detail: (1) the Zambezi river basin in South Africa and (2) the Sahara desert. The Zambezi River basin is the fourth-largest basin of Africa, after the Congo/Zaire, Nile and Niger basins (see Fig. 13). The basin has a strong annual amplitude of more than 15 cm equivalent water height. Its total area is about 1.4 million km^2. For the Zambezi River basin, a Lumped Elementary Watershed (LEW) regional hydrological model is used as reference. The LEW approach has been presented in a previous study by Winsemius *et al.* (2006) (see also Klees *et al.* 2007). The part of

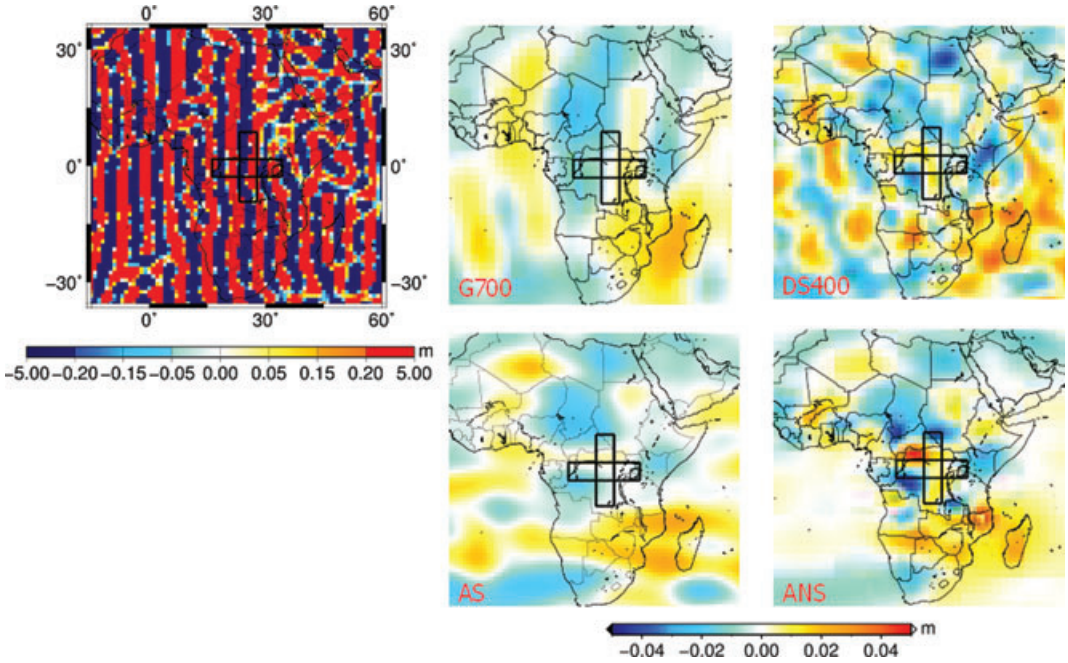

Figure 11. Noise before (left-hand upper panel) and after filtering over South Africa. 700 km isotropic Gaussian filter (G700), convolution of destriping filter and 400 km isotropic Gaussian filter (DS400), optimal AS filter (AS) and optimal ANS filter (ANS). Strong residual noise patterns of amplitudes up to 4 cm and constant sign over areas as large as 10^6 km^2 are evident in the DS400, optimal AS and optimal ANS solutions.

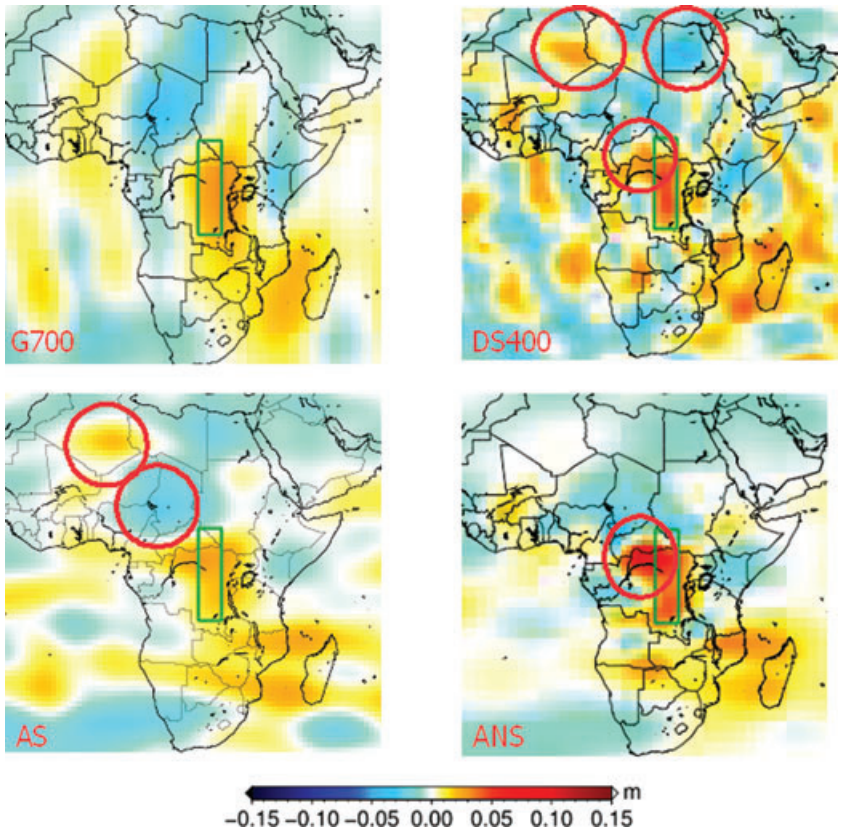

Figure 12. Signal and noise after filtering. Several local residual noise features are highlighted by red circles. The green box indicates the area of a 10 cm water mass layer, which is the (true) mass change signal. Hence, every signal outside the green box is due to residual noise or leakage. From left- to right-hand side: 700 km isotropic Gaussian filter (G700), convolution of destriping filter and 400 km isotropic Gaussian filter (DS400), optimal AS filter (AS) and optimal ANS filter (ANS).

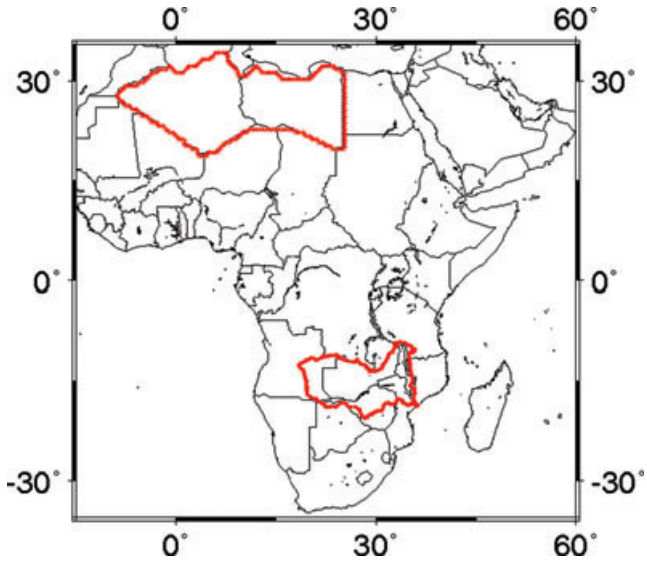

Figure 13. The Zambezi river basin and the part of the Sahara desert used in the study.

the Sahara desert being used in this study comprises only the driest part of the desert. In particular, the Nile River basin in the eastern part and the Atlas mountain range in the western part of the Sahara desert have been excluded (see Fig. 13). The area extends over about 3.5 million km^2 and will be referred to as Sahara desert for simplicity. When accepting that the monthly mean water storage variations over this area are almost zero, then the GRACE estimates represent residual noise artefacts and/or leakage from surrounding areas, in particular from the Mediterranean Sea, the Intertropical Convergence Zone, and the Nile River basin.

Fig. 14 shows geographical plots of mass change for 2005 April derived from GRACE KBR data using the methodology developed at DEOS (Ditmar & Liu 2006). A comparison of the filtered solutions reveal some interesting differences. First, we observe that the optimal ANS filter seems to preserve significantly more signal and shows less pronounced leakage effects. Examples of areas where this effect is clearly visible are Antartica, the Amazon River basin, the Chukchi Peninsula (the northeastern extremity of Asia in the northern part of the Russian Far East), Madagaskar, and Scandinavia. For instance, ANS is the only filter, which shows a clear mass change signal on Madagaskar and the Chukchi Peninsula; the latter is probably caused by strong snow cover. This mass change signal is not visible in the G700, AS, and DS400 solutions, which is likely due to leakage effects. Second, the ANS filter provides the smoothest solution over the oceans. This is explained by the fact that mass redistribution over most of the oceans is much smaller than over land. Therefore, the optimal ANS filter, which uses information about signal and noise variances and covariances, applies a stronger smoothing to areas of low signal-to-noise ratio.

Fig. 15 shows geographical plots of mass change for 2005 April after filtering compared with the unfiltered output of the LEW regional hydrological model. The plots indicate that the optimal ANS filter is the closest to LEW among all filters. The optimal AS filter performs pretty well, which may be explained by the dominating east–west mass change features. DS400 and G700 perform worse. For DS400 this may be explained by the enhanced noise in equatorial regions, which is not filtered out sufficiently well when destriping, and by the successive application of an isotropic 400 km Gaussian filter. The superior performance of the ANS filter is confirmed when looking at the mean water mass change over the Zambezi basin for the period 2003 February till 2006 February (Fig. 16). The largest differences between LEW and filtered GRACE solutions occur during periods of extreme water mass change. ANS is always closer to LEW than any other filter is, for example, for 2004 April, 2004 October and 2005 April. The better performance of the optimal ANS filter is also confirmed by the RMS fit to LEW over a 3-yr time period (see Fig. 16).

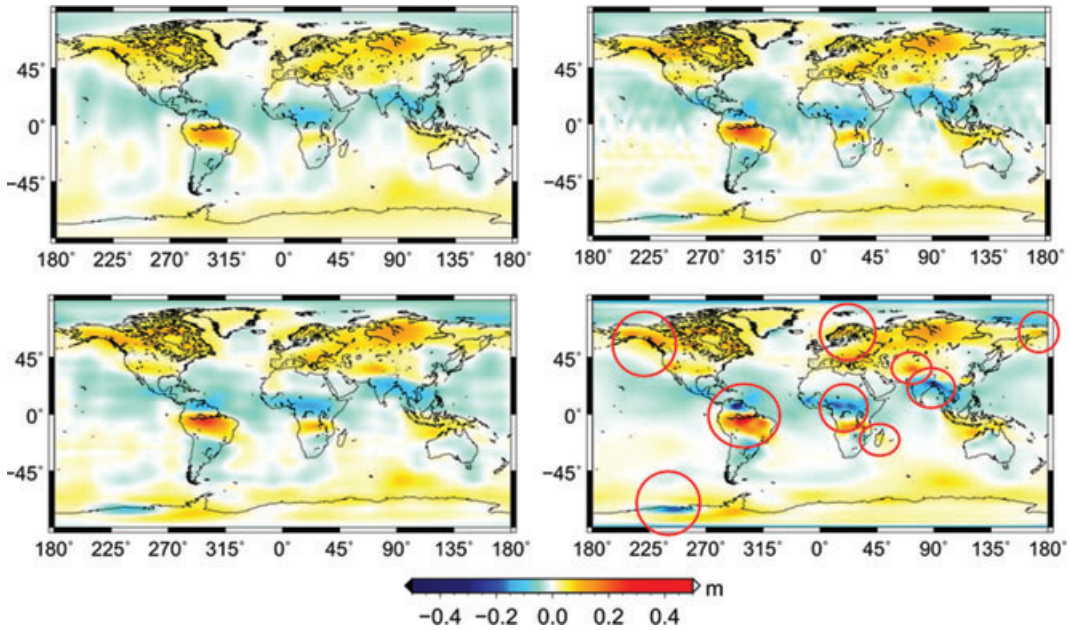

Figure 14. Mass change for 2005 April from GRACE KBR data after filtering. Units are in [m] equivalent water height. 700 km isotropic Gaussian filter (G700, left-hand upper panel), convolution of destriping filter and 400 km isotropic Gaussian filter (DS400, right-hand upper panel), optimal AS filter (AS, left-hand lower panel) and optimal ANS filter (ANS, right-hand lower panel). The ANS filter preserves more signal, shows less pronounced leakage, and provides a smoother solution over the oceans. Some of these areas are marked by red circles.

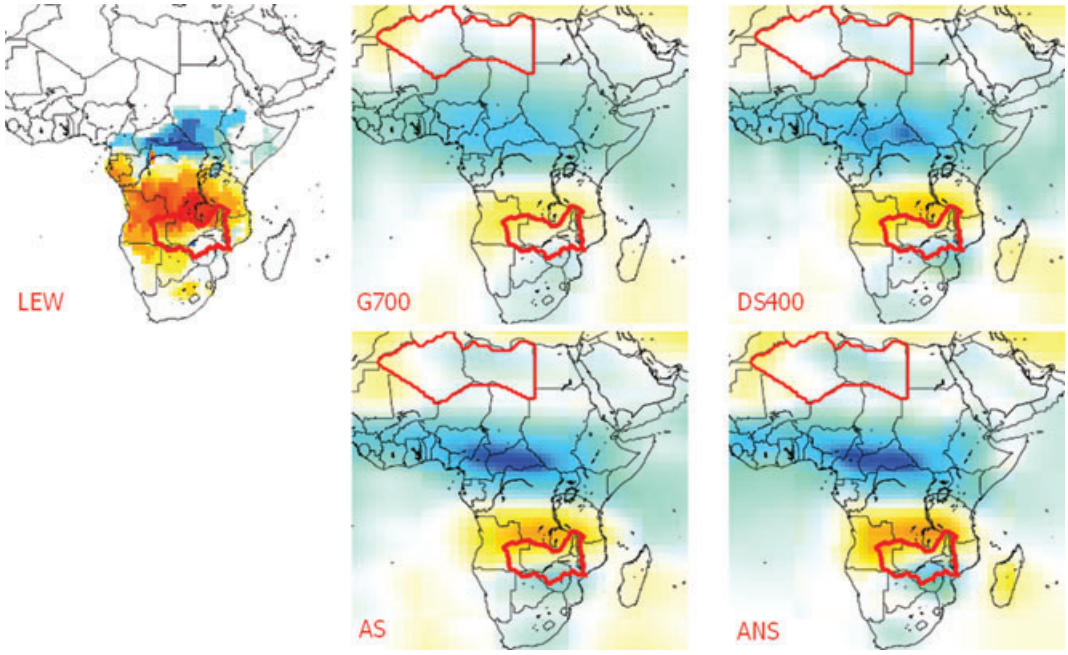

Figure 15. Surface mass change in equivalent water height for 2005 April. Output of the LEW regional hydrological model (LEW) and GRACE solutions after application of various filters: 700 km isotropic Gaussian filter (G700), convolution of destriping filter and 400 km isotropic Gaussian filter (DS400), optimal AS filter (AS) and optimal ANS filter (ANS).

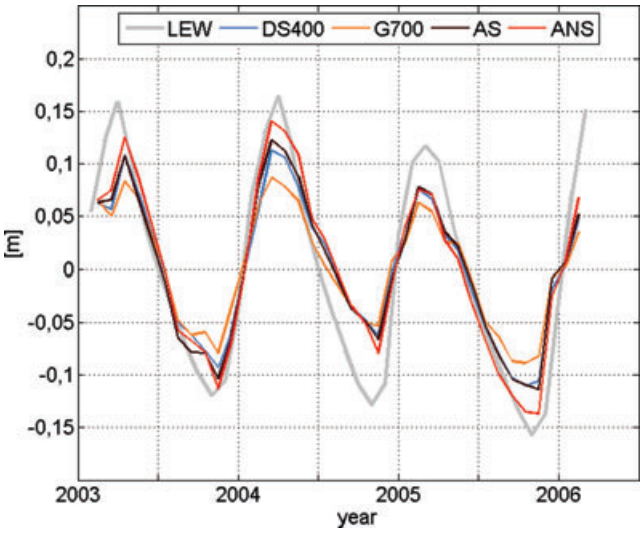

Figure 16. Mean water mass change over the Zambezi river basin from 2003 February till 2006 February. Units are in [m] of equivalent water height. Output of the LEW regional hydrological model (LEW) and GRACE solutions after application of various filters: 700 km isotropic Gaussian filter (G700), convolution of destriping filter and 400 km isotropic Gaussian filter (DS400), optimal AS filter (AS) and optimal ANS filter (ANS). The RMS difference with respect to the LEW model are 0.049, 0.041, 0.039 and 0.034 m, respectively.

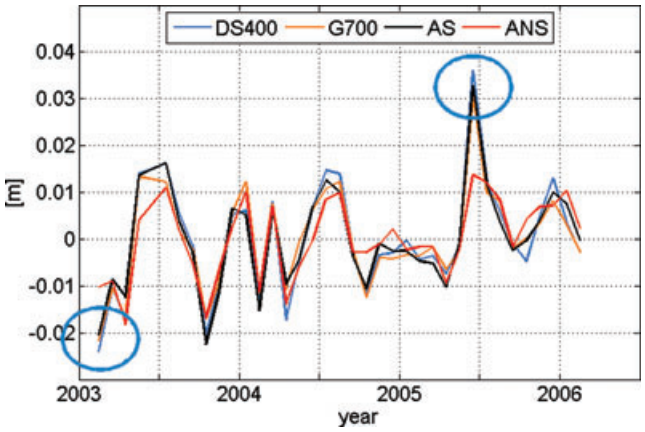

Figure 17. Monthly mean water mass change over the Sahara desert for the period 2003 February till 2006 February. 700 km isotropic Gaussian filter (G700), convolution of destriping filter and 400 km isotropic Gaussian filter (DS400), optimal AS filter (AS) and optimal ANS filter (ANS).

We performed similar computations for the driest part of the Sahara desert, with the assumption that the signal is close to zero over this region. If the assumption is valid, everything seen in this area is the effect of residual noise and leakage from surrounding areas. A 3-yr time-series of the mean water mass change over this part of Sahara desert (see Fig. 17) reveals some remarkable differences between the optimal ANS filter and the other filters. The latter indicate a strong mass change in 2003 February and 2005 June, whereas ANS does not. Fig. 18 shows the four solutions for 2005 June. The G700, AS and DS400 solutions show a relatively strong mass change signal at the centre of the Sahara desert, which is much less pronounced in the ANS solution. A possible explanation is that we have to deal with a noise artefact, which is successfully suppressed by the optimal ANS filter, because the signal-to-noise ratio in this area is very small. Note that noise artefacts in the Sahara desert of similar pattern and size have been observed as well in the simulation scenarios of Section 4, Fig. 12. Another explanation is that we have to deal with an episodic signal, which is falsely filtered out by the optimal ANS filter, but well recovered by the other filters. Episodic signals are hard to detect by the optimal ANS filter as it is currently implemented, because the signal variance–covariance matrix is built up using spatial-domain signal variances obtained from a 3-yr time-series of GRACE solutions. Hence, an episodic event will

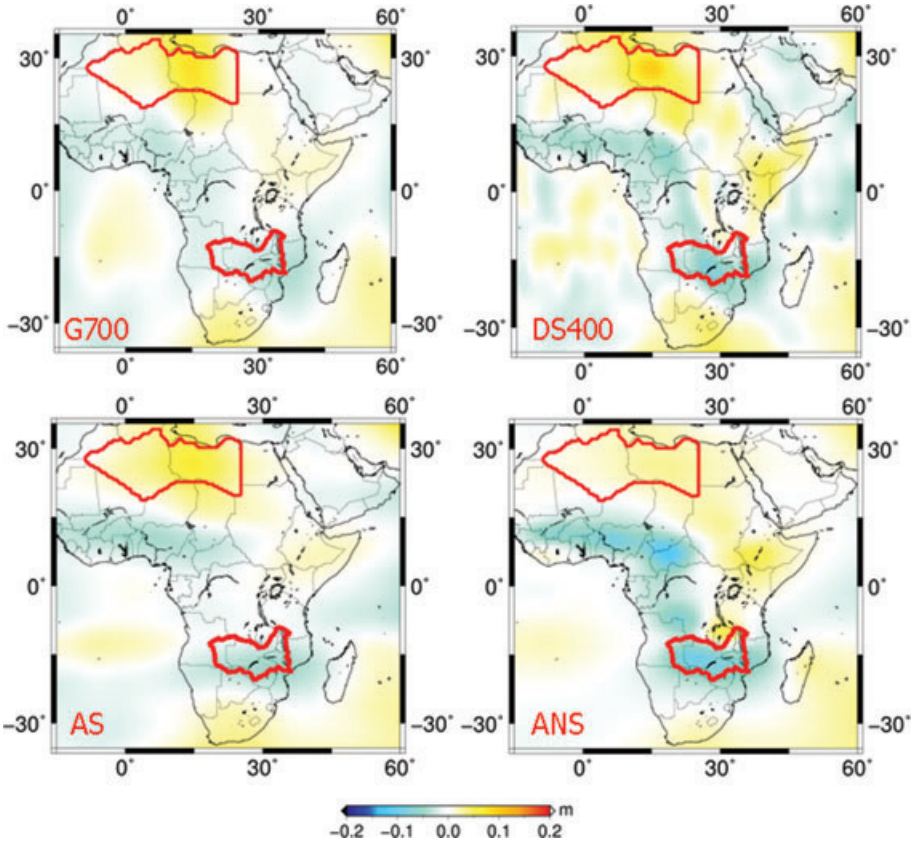

Figure 18. Mean water mass change over the Sahara desert for 2005 June after the application of various filters: 700 km isotropic Gaussian filter (G700), convolution of destriping filter and 400 km isotropic Gaussian filter (DS400), optimal AS filter (AS) and optimal ANS filter (ANS). Note the strong mass change signal at the centre of the Sahara desert visible in the G700, DS400 and AS solutions, which is almost absent in the ANS solution.

always be underestimated in the signal variance–covariance matrix, which means that the ANS filter filters-out this event because of the low signal-to-noise ratio.

Overall, the optimal ANS filter provides the smallest RMS signal over a time span of 3 yr: 0.8 cm compared with 1 cm (G700), 1.1 cm (optimal AS) and 1.2 cm (DS400).

6 SENSITIVITY ANALYSIS

The results of the simulation scenarios and the real data scenarios have shown that the optimal ANS filter performs better than any other filter tested in this study. The optimal ANS filter, however, requires information about the noise variances and covariances, and the signal variances and covariances. Our strategy to set-up the signal variance–covariance matrix requires only information, which is available to everybody. The situation is different for the noise variance–covariance matrices. In our study, we used the matrices as they came out of the least-squares adjustment of GRACE KBR data according to the methodology developed at DEOS. Similar filtering could be done by the others centres which process GRACE KBR data. For the majority of the users, however, only information about the noise variances is available. Hence, they cannot implement the optimal ANS filter. Therefore, from a practical point of view, it is interesting to gain some insight into the sensitivity of the optimal ANS filter with respect to approximations of the noise variance–covariance matrix, which is the main question to be addressed in this section. Moreover, we will also look into the sensitivity with respect to approximations of the signal variance–covariance matrix.

Four simplified ANS-filters will be investigated.

(i) The noise covariances are neglected and the signal variance–covariance matrix is left unchanged (ANS-1).

(ii) Noise correlations are computed following the approach of Kusche (2007) and scaled by a single scale factor to match the noise degree variances of the DEOS noise variance–covariance matrix as well as possible; the signal variance–covariance matrix is left unchanged (ANS-2). Fig. 19 shows the noise degree variances obtained in this way.

(iii) Noise correlations are computed following the approach of Kusche (2007) and scaled to the variances of the full noise variance–covariance matrix, which is used in the optimal ANS filter (ANS-3).

(iv) Full noise variance–covariance matrix is used; the signal covariances are neglected (ANS-4).

Fig. 20 shows the differences between the optimal ANS-filter solution for 2005 April and the corresponding GRACE solutions filtered with the approximate ANS-filters. The worst solution is the ANS-4 solution, which neglects the signal covariances. Differences with respect to the optimal ANS solution attain values of up to 11 cm in terms of equivalent water heights, which is about 25 per cent of the maximum signal amplitudes. Taking the full signal variance–covariance matrix into account and using a synthetic noise covariance matrix as proposed by Kusche (2007) improves the quality significantly provided that the covariance matrix is properly scaled. Scaling it to match estimated noise degree variances (ANS-2) as proposed by Kusche (2007) introduces errors that are a factor of 2 larger than a scaling to the estimated noise variances

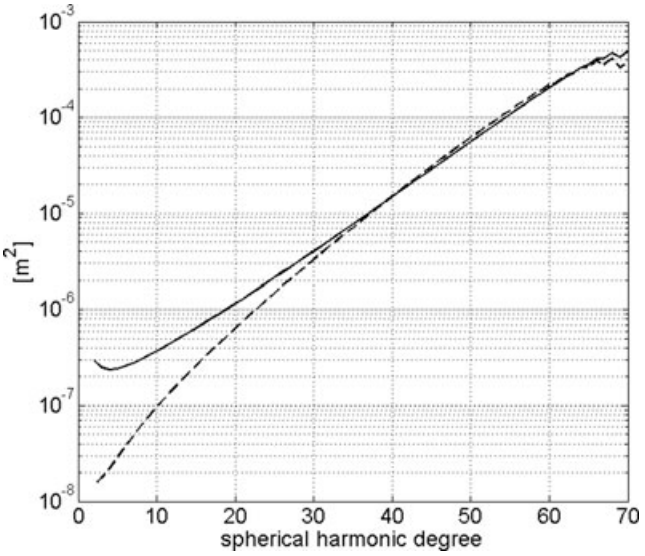

Figure 19. Mean noise variances per coefficient (1) from the noise variance–covariance matrix of the DEOS GRACE solution for 2005 April (solid line); (2) according to the approach of Kusche (2007) when applying a single scale factor to match the upper tail of (1) as good as possible (dashed line). The latter have been used to design the ANS-2 filter. Units are in (m) of equivalent water height.

(i.e. to the diagonal elements of the inverse normal equation matrix) (ANS-3). The quality of the ANS-2 solution is only slightly better than the quality of the ANS-1 solution, which neglects noise covariances. Note that it does not matter how the estimated noise degree variances are obtained; either from given estimated noise variances or using the increasing branch (above degree, say, 30) of the average power per degree of monthly GRACE solutions over several years, as used in (Kusche 2007).

7 CONCLUSIONS

We have proposed a new filter which takes signal and noise covariances into account. The filter is optimal in the sense that it minimizes the global mean of the square difference between the signal and the filtered GRACE estimate among all possible anisotropic non-symmetric filters. A series of simulations and computations with real data has shown that this filter performs significantly better than, for instance, the convolution of destriping and Gaussian filter, all anisotropic symmetric filters, or all isotropic filters. The optimal ANS filter preserves the signal amplitudes better, has a smaller leakage error (e.g. along the coast), and provides smoother solutions in areas of low signal (e.g. oceans). The filter relies upon full noise and signal variance–covariance matrices. Neglecting noise and/or signal covariances degrades the filter performance significantly. Neglecting signal covariances has the largest effect on the filter performance

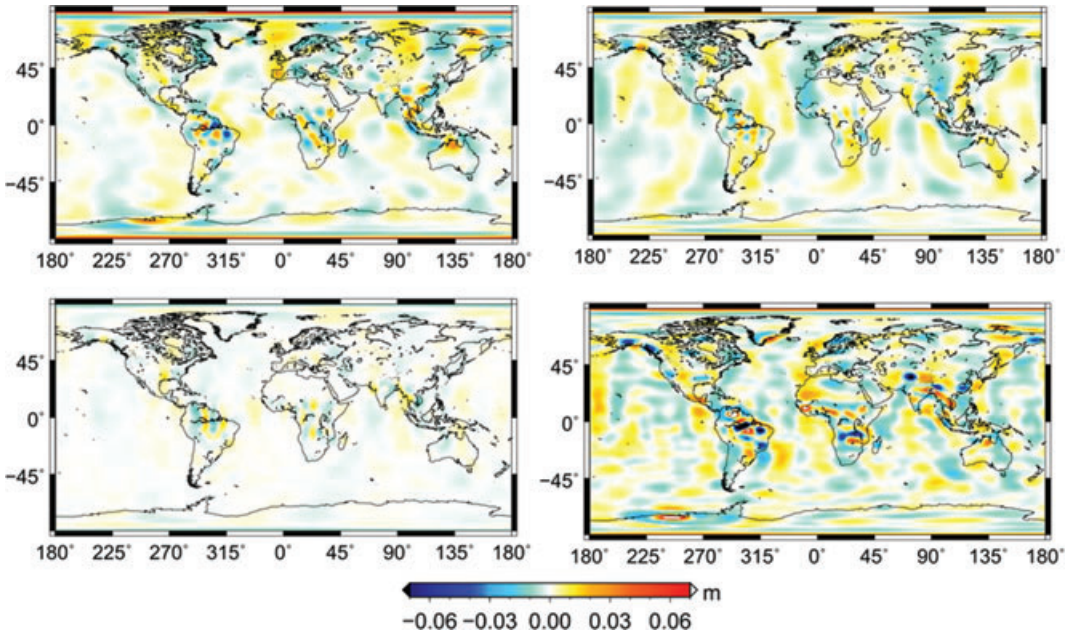

Figure 20. Differences between the optimal ANS-filter solution for 2005 April and various ANS-filter approximations. Units are in (m) of equivalent water height. Noise covariances are neglected and full signal variance–covariance matrix is used (ANS-1, left-hand upper panel); full signal variance–covariance matrix is used and the synthetic noise correlations, which are obtained by following the approach of Kusche (2007), are scaled by a single scale factor to the noise signal degree variances (ANS-2, right-hand upper panel); full signal variance–covariance matrix is used and the synthetic noise correlations, which are obtained by following the approach of Kusche (2007), are scaled to the noise variances from the DEOS 2005 April noise variance–covariance matrix (ANS-3, left-hand lower panel); full noise variance–covariance matrix is used and signal covariances are neglected (ANS-4, right-hand lower panel). Obviously, neglecting the signal covariances has the largest effect on the solution (ANS-4). Note that the differences shown in the bottom right-hand panel attain values up to 11 cm, which are outside the interval represented by the colour bar.

and should be avoided. The effect of neglecting noise covariances is lower (for 2005 April by a factor of 2), though still significant. If no noise variance–covariance information is available, the user can generate a noise correlation matrix following the approach proposed by Kusche (2007); however, the matrix should be properly scaled using information about the noise variances, which is part of the official level 2 products of the GRACE processing teams at the CSR, GFZ and JPL. A scaling using noise degree variances should be avoided because it degrades the filter performance.

A further improvement of the ANS filter is possible if one succeeds in computing a more realistic signal variance–covariance matrix. An even better performance can be expected from a joint inversion of GRACE KBR data or gravity models and mass redistribution information provided by geophysical models. This requires a realistic description of the uncertainty of the geophysical models, which is hardly available today. Without this information, the result of the inversion could be biased towards the geophysical models or would not differ significantly from a GRACE-only solution.

ACKNOWLEDGMENTS

We wish to thank J.L. Chen, S.-C. Han and one anonymous reviewer for their criticisms and corrections, which helped us to improve the manuscript.

REFERENCES

Chen, J.L., Wilson, C.R. & Seo, K.-W., 2006. Optimized smoothing of gravity recovery and climate experiment (GRACE) time-variable gravity observations, *J. geophys. Res.,* **111,** B06408, doi:10.1029/2005JB004064.

Davis, J.L., Tamisiea, M.E., Elósegui, P., Mitrovica, J.X. & Hill, E.M., 2008. A statistical filtering approach for Gravity Recovery and Climate Experiment (GRACE) gravity data, *J. geophys. Res.,* **113,** B04410, doi:10.1029/2007JB005043.

Ditmar, P. & Liu, X., 2006. Gravity field modeling on the basis of GRACE Range-Rate combinations: current results and challenge, in *Proceedings of the First International Symposium of the International Gravity Field Service (IGFS)*, 28 August–1 September, 2006, Istanbul, Turkey.

Ditmar, P., Kusche, J. & Klees, R., 2003. Computation of spherical harmonic coefficients from satellite gravity gradiometry data to be acquired by the GOCE satellite: regularization issues, *J. Geod.,* **77,** 465–477.

Freeden, W., Gervens, T. & Schreiner, M., 1998. Constructive approximations on the sphere (with applications to geomathematics), Oxford Sciences Publication, Clarendon Press, Oxford University.

Fukumori, I., Lee, T., Menemenlis, D., Fu, L.I., Cheng, B., Tang, B., Xing, Z. & Giering, R., 2000. A dual assimilation system for satellite altimetry, paper presented at joint TOPEX/Poseidon and Jason-1 Science Working Team Meeting, Univ. Corp. for Atmos. Res., Miami Beach, Florida.

Han, S.-C. & Ditmar, P. 2008. Localized spectral analysis of global satellite gravity fields for recovering time-variable mass redistributions, *J. Geod.,* **82,** 423–430.

Han, S.-C. & Simons, F.J., 2008. Spatiospectral localization of global geopotential fields from the Gravity Recovery and Climate Experiment (GRACE) reveals the coseismic gravity change owing to the 2004 Sumatra-Andaman earthquake, *J. geophys. Res.,* **113,** B01405, doi:10.1029/2007JB004927.

Han, S.-C., Shum, C.K., Jekeli, C., Kuo, C.-Y., Wilson, C.R. & Seo, K.-W., 2005. Non-isotropic filtering of GRACE temporal gravity for geophysical signal enhancement, *Geophys. J. int.,* **163,** 18–25.

Healy, D., Rockmore, D., Kostelec, P. & Moore, S., 2003. FFTs for the 2-sphere—improvements and variations, *J. Fourier Anal. Appl.,* **9,** 341–385.

Klees, R., Zapreeva, E.A., Winsemius, H.C. & Savenije, H.H.G., 2007. The bias in GRACE estimates of continental water storage, *Hydrol. Earth Syst. Sci.,* **11,** 1227–1241.

Kusche, J., 2007. Approximate decorrelation and non-isotropic smoothing of time-variable GRACE-type gravity field models, *J. Geod.,* **81,** 733–749.

Milly, P.C.D. & Shmakin, A.B., 2002. Global modeling of land water and energy balances, Part I: the land dynamics (LaD) model, *J. Hydrometerol.,* **3,** 283–299.

Lemoine, F.G., Luthcke, S.B., Rowlands, D.D., Chinn, D.S., Klosko, S.M. & Cox, C.M., 2007. The use of mascons to resolve time-variable gravity from GRACE, in *Dynamic Planet: Monitoring and Understanding a Dynamic Planet with Geodetic and Oceanographic Tools, International Association of Geodesy Symposia*, Vol. 130, pp. 231–236, eds Tregoning, P. and Rizos, C., Springer, Berlin.

Rodell, M., Famiglietti, J.S., Chen, J., Seneviratne, S.I., Viterbo, P., Holl, S. & Wilson, C.R., 2004. Basin scale estimates of evapotranspiration using GRACE and other observations, *Geophys. Res. Lett.,* **31,** L20504, doi:10.1029/2004GL020873.

Rowlands, D.D., Luthcke, S.B., Klosko, S.M., Lemoine, F.G.R., Chinn, D.S., McCarthy, J.J., Cox, C.M. & Anderson, O.B., 2005. Resolving mass flux at high spatial and temporal resolution using GRACE intersatellite measurements, *Geophys. Res. Lett.,* **32,** L04310, doi:10.1029/2004GL021908.

Sasgen, I., Martinec, Z. & Fleming, K., 2006. Wiener optimal filtering of GRACE data, *Stud. Geophys. Geod.,* **50,** 499–508.

Savitzky, A. & Golay, M.J.E., 1964. Smoothing and differentiation of data by simplified least squares procedures, *Anal. Chem.,* **36,** 1627–1639.

Seo, K.-W., Wilson, C.R., Famiglietti, J.S., Chen, J.L. & Rodell, M., 2006. Terrestrial water mass load changes from gravity recovery and climate experiment (GRACE), *Water Resour. Res.,* **42,** W05417, doi:10.1029/2005WR004255.

Swenson, S. & Wahr, J., 2002. Methods for inferring regional surface-mass anomalies from gravity recovery and climate experiment (GRACE) measurements of time-variable gravity, *J. geophys. Res.,* **107**(B9), 2193, doi:10.1029/2001JB000576, 2002.

Swenson, S. & Wahr, J., 2006. Post-processing removal of correlated errors in GRACE data, *Geophys. Res. Lett.,* **33,** L08402, doi:10.1029/2005GL025285.

Velicogna, I. & Wahr, J., 2006. Measurements of time-variable gravity shows mass loss in Antarctica, *Science,* **311,** no. 5768, 1754–1756.

Wahr, J., Molenaar, M. & Bryan, F., 1998. Time variability of the earth's gravity field: hydrological and oceanic effects and their possible detection using GRACE, *J. geophys. Res.,* **108**(B12), 30 205–30 229.

Winsemius, H.C., Savenije, H.H.G., Gerrits, A.M.J., Zapreeva, E.A. & Klees, R., 2006. Comparison of two model approaches in the Zambezi river basin with regard to model confidence and identifiability, *Hydrol. Earth Syst. Sci.,* **10,** 339–252.

Wouters, B. & Schrama, E.J.O., 2007. Improved accuracy of GRACE gravity solutions through empirical orthogonal function filtering of spherical harmonics, *Geophys. Res. Lett.,* **34,** L23711, doi:10.1029/2007GL032098.

APPENDIX A: MINIMUM MSE

We want to show that the minimum of

$$\mathrm{MSE}_{\mathrm{ave}} = \frac{1}{4\pi R^2} \int_{\sigma_R} E\{(f - \hat{f}_w)^2\}\, \mathrm{d}\sigma_R, \tag{A1}$$

is attained if

$$\mathbf{W} = \mathbf{D}\,(\mathbf{C} + \mathbf{D})^{-1}, \tag{A2}$$

where $\mathbf{W} = (W_{lm,pq})$ is the filter matrix, $\mathbf{C}$ is the full noise variance–covariance matrix of the Stokes coefficients of the estimated mass change function $\hat{f}$ and $\mathbf{D}$ is the full frequency-domain signal variance–covariance matrix. We define vectors

$$\mathbf{y}(x) = [Y_{l,m}(\hat{x})] \tag{A3}$$

$$\mathbf{c}^{(\cdot)} = (\bar{c}^{(\cdot)}_{l,m}) \tag{A4}$$

$$\mathbf{w}_{l,m} = (W_{lm,pq}). \tag{A5}$$

Then, we can write in matrix–vector notation,

$$f(x) - f_w(x) = \mathbf{y}^T(x)\,\mathbf{c}^{(f)} - \mathbf{y}^T(x)\,\mathbf{W}\,\mathbf{c}^{(f)} \tag{A6}$$

$$= \mathbf{y}^T(x)(\mathbf{I} - \mathbf{W})\,\mathbf{c}^{(f)} \tag{A7}$$

$$f_w(x) - \hat{f}_w(x) = \mathbf{y}^T(x)\,\mathbf{W}\,\mathbf{c}^{(f)} - \mathbf{y}^T(x)\,\mathbf{W}\,\mathbf{c}^{(\hat{f})} \tag{A8}$$

$$= \mathbf{y}^T(x)\,\mathbf{W}\,\mathbf{c}^{(\varepsilon_f)}, \tag{A9}$$

where $\mathbf{c}^{(\varepsilon_f)} = \mathbf{c}^{(f)} - \mathbf{c}^{(\hat{f})}$. The mean-square error is

$$\mathrm{MSE} = (f - f_w)^2 + E\left[(f_w - \hat{f}_w)^2\right]. \tag{A10}$$

It is

$$(f - f_w)^2 = \mathbf{y}^T(x)[(\mathbf{I} - \mathbf{W})\mathbf{D}(\mathbf{I} - \mathbf{W})^T]\mathbf{y}(x), \tag{A11}$$

where $\mathbf{D} = \mathbf{c}^{(f)}\,[\mathbf{c}^{(f)}]^T$, and

$$E\left[(f_w - \hat{f}_w)^2\right] = \mathbf{y}^T(x)\,\mathbf{W}\mathbf{C}\mathbf{W}^T\,\mathbf{y}(x), \tag{A12}$$

where $\mathbf{C} = E\{\mathbf{c}^{(\varepsilon_f)}[\mathbf{c}^{(\varepsilon_f)}]^T\}$. Using the equations for $(f - f_w)^2$ and $E\left[(f_w - \hat{f}_w)^2\right]$, we find

$$\mathrm{MSE}(x) = \mathbf{y}^T(x)\left[(\mathbf{I} - \mathbf{W})\mathbf{D}(\mathbf{I} - \mathbf{W})^T + \mathbf{W}\mathbf{C}\mathbf{W}^T\right]\mathbf{y}(x). \tag{A13}$$

The global mean of the MSE attains a minimum if the term inside $[\cdot]$ attains a minimum. Hence, a necessary condition for a minimum of $\mathrm{MSE}_{\mathrm{ave}}$ is

$$\frac{\partial}{\partial \mathbf{W}}\left[(\mathbf{I} - \mathbf{W})\mathbf{D}(\mathbf{I} - \mathbf{W})^T + \mathbf{W}\mathbf{C}\mathbf{W}^T\right] = \mathbf{0}, \tag{A14}$$

or

$$-2\mathbf{D} + 2(\mathbf{D} + \mathbf{C})\,\mathbf{W}^T = \mathbf{0} \Rightarrow \mathbf{W} = \mathbf{D}\,(\mathbf{C} + \mathbf{D})^{-1}. \tag{A15}$$

The positive definiteness of $\mathbf{C} + \mathbf{D}$ guarantees that $\mathrm{MSE}_{\mathrm{ave}}$ attains a minimum at $\mathbf{W} = \mathbf{D}(\mathbf{C} + \mathbf{D})^{-1}$. Eq. (A15) is identical with eq. (4).